Bioactive Materials 20 (2023) 368–380

Contents lists available at ScienceDirect

Bioactive Materials

journal homepage: www.keaipublishing.com/en/journals/bioactive-materials

# Rationally designed bioactive milk-derived protein scaffolds enhanced new bone formation

Min Suk Lee [a,b,1], Jin Jeon [a,1], Sihyeon Park [a], Juhan Lim [a], Hee Seok Yang [a,c,*]

[a] Department of Nanobiomedical Science & BK21 FOUR NBM Global Research Center for Regenerative Medicine, Dankook University, Cheonan, 31116, Republic of Korea
[b] Medical Laser Research Center, College of Medicine, Dankook University, Cheonan, 31116, Republic of Korea
[c] Center for Bio-Medical Engineering Core-Facility, Dankook University, Cheonan, 31116, Republic of Korea

ARTICLE INFO

*Keywords:*
Casein
Bioactive peptides
Bone regeneration
Protein based scaffold
Physical crosslinking

ABSTRACT

Recently, a number of studies reported that casein was composed of various multifunctional bioactive peptides such as casein phosphopeptide and β-casochemotide-1 that bind calcium ions and induce macrophage chemotaxis, which is crucial for bone homeostasis and bone fracture repair by cytokines secreted in the process. We hypothesized that the effects of the multifunctional biopeptides in casein would contribute to improving bone regeneration. Thus, we designed a tissue engineering platform that consisted of casein and polyvinyl alcohol, which was a physical-crosslinked scaffold (milk-derived protein; MDP), via simple freeze-thaw cycles and performed surface modification using 3,4-dihydroxy-L-phenylalanine (DOPA), a mussel adhesive protein, for immobilizing adhesive proteins and cytokines for recruiting cells in vivo (MDP-DOPA). Both the MDP and MDP-DOPA groups proved indirectly contribution of macrophages migration as RAW 264.7 cells were highly migrated toward materials by contained bioactive peptides. We implanted MDP and MDP-DOPA in a mouse calvarial defect orthotopic model and evaluated whether MDP-DOPA showed much faster mineral deposition and higher bone density than that of the no-treatment and MDP groups. The MDP-DOPA group showed the accumulation of host M2 macrophages and mesenchymal stem cells (MSCs) around the scaffold, whereas MDP presented mostly M1 macrophages in the early stage.

## 1. Introduction

The bone restoration process, which involves various progenitor cells such as inflammatory, endothelial, and hematopoietic cells, has three distinct phases, the inflammation phase, the reparative phase, and the osteogenesis or new bone formation phase [1]. In the inflammation phase, tissue-resident and infiltrating macrophages are initially recruited and secrete pro-inflammatory cytokines at the fractured bone areas [2]. M1 phenotype macrophages, which are activated by the cytokines maintain the pro-inflammatory state by secreting interferon-γ (IFN γ), tumor necrosis factor-α (TNFα), and interleukin-2 (IL-2) signals. However, if an excessive immune response occurs, tissue repair is delayed without moving on to the next healing phase [3]. After then, overlapped at that phase, selectively triggered M2 phenotype macrophages hinder the inflammatory response by secreting anti-inflammatory cytokines such as IL-4, IL-10, and IL-1Rα and play a crucial role in healing fractured area by promoting recruitment of bone marrow mesenchymal stem cells (bmMSCs) and the secretion of transforming growth factor-β (TGF-β), osteopontin (OPN) and bone morphogenic protein-2 (BMP2) [4]. For these reasons, adopting a strategy for bone fracture repair that modulates a shift from the inflammatory to the anti-inflammatory phases seems reasonable. However, we paid attention to the sequential events, where if many macrophages were recruited to the defect site in the early stage, chemotaxis created by the cytokines secreted from the recruited host cells would cause the rapid accumulation of osteogenic progenitor cells.

To modulate artificial immune responses for recruiting macrophages, several cytokines such as IL-17 [5] and TNFα have been directly

Peer review under responsibility of KeAi Communications Co., Ltd.
* Corresponding author. Department of Nanobiomedical Science & BK21 FOUR NBM Global Research Center for Regenerative Medicine, Dankook University, Cheonan, 31116, Republic of Korea.
*E-mail address:* hsyang@dankook.ac.kr (H.S. Yang).
[1] These authors contributed equally.

https://doi.org/10.1016/j.bioactmat.2022.05.028
Received 21 February 2022; Received in revised form 9 May 2022; Accepted 23 May 2022

applied [6], but these cytokines have also shown dose-dependent side effects such as an increased risk of severe osteoclastogenesis and rheumatoid arthritis development, Th17-dependent autoimmune responses, and prolonged inflammation [7]. In addition, bioceramics with various bioactive ions or surface topography have been used as biomedical implant scaffold materials to modulate immune responses in the host. However, some bioceramics or ions induced inappropriate excessive inflammatory responses, which were a great hindrance for the bone healing process, and the mechanism by which the surface topography modulated the immune response is not fully understood [8–10]. Based on these immune responses in the body, we tried to find the appropriate bioactive biomaterials to safely boost the recruitment of macrophages in a biological environment. Bioactive proteins from food, as well as casein protein, which account for 80% of the proteins in milk, have demonstrated that various kinds of biologically active peptides could have immunostimulant, antithrombotic, antioxidative functions, and other health-promoting effects [11] and are generally recognized as safe (GRAS), meaning that they are biocompatible with biological environments [12]. We focused on two specific bioactive peptides in casein, casein phosphopeptide (CPP) and β-casochemotide-1, for effective bone regeneration. Many studies have been shown that CPP has acidic motifs, which is a negatively charged region, for binding calcium ions [13] and induces excellent osteogenic activity in osteoblasts [14]. β-casochemotide-1 has also been reported to promote macrophage migration by promoting a high level of chemotaxis [15]. Using the beneficial effects of these bioactive peptides in casein as a tissue engineering platform, we attempted to investigate whether the calcium-binding affinity and chemotactic activity of recruited host macrophages by bioactive peptides would contribute to the induction of bone regeneration.

To prepare a bone tissue engineering platform using milk-derived protein casein, we applied poly (vinyl alcohol) (PVA), which is a Food and Drug Administration (FDA)-approved biocompatible synthetic polymer, to induce physically cross-linked scaffolds (MDPs) through freeze-thaw cycles [16] without any chemical cross-linking agents that could cause subtle changes in the primary structure of casein [17]. Furthermore, to improve the attachment of recruited host cells to the fabricated scaffold, we modified the surface of the MDP scaffold using 3, 4-dihydroxy-L-phenylalanine (DOPA), a mussel adhesive protein (MDP-DOPA). In this study, we investigated the surface characteristics of MDP and MDP-DOPA scaffolds using various analyses and examinations to determine whether the bioactive protein scaffolds could recruit macrophages to the materials under in vitro and in vivo conditions. We also performed an in vivo animal study using a mouse calvarial defect model and measured the extent to which the implanted scaffolds could heal the defected areas through live micro-computed tomography (CT) and histological analysis. Furthermore, we verified which types of macrophages and cytokines were recruited and secreted respectively at the defect area by scaffolds in the early stage in an in vivo animal study.

## 2. Materials and methods

### 2.1. Preparation of milk-derived protein scaffolds

The MDP and MDP-DOPA scaffolds were prepared using the freeze-thaw method. Briefly, 1.0 g of bovine casein (Sigma-Aldrich) was dissolved in 12.5 mL of 1 M sodium hydroxide (DAEJUNG, Gyeonggi-do, Korea) and 0.5 g of PVA (Sigma-Aldrich) was dissolved in 12.5 mL of distilled water (DW). These solutions were gently mixed for 1 h on a stirring machine (Corning) and dispensed onto cell culture plates (Corning) at 10 mL. The culture plates underwent freeze-thawing by freezing at −80 °C (OPERON, Gyeonggi-do, Korea) for 4 h and thawing at room temperature for 2 h. The freeze-thaw cycles were repeated at least 3 times. Casein and PVA were physically cross-linked to form scaffolds by the freeze-thaw cycles. These scaffolds were freeze-dried and stored at −80 °C. MDP was modified by DOPA (Sigma-Aldrich) to improve surface hydrophilicity for the attachment and invasion of host cells. MDP was immersed and shaken in Tris buffer (10 mM, pH 8.5, Sigma-Aldrich) containing DOPA (2 mg/mL) at room temperature for 16 h. The MDP-DOPA scaffold was washed to remove non-oxidized DOPA and freeze-dried for further studies.

### 2.2. Characterization of the MDP and MDP-DOPA

The surface analysis of MDP and MDP-DOPA was conducted by fixing on a stub using carbon double-sided tape (Nisshin) and sputter-coated with platinum at a plasma current of 30 mA for 100 s under a vacuum to a thickness of 5 nm using a sputter coater (Sputter Coater 108 Auto, Cressington, Watford, UK). The MDP and MDP-DOPA scaffolds (n = 3/per group) were characterized by scanning electron microscopy (SEM, JEOL, Tokyo, Japan) at an accelerating voltage of 20 kV. The DOPA-coated MDP scaffold was investigated using X-ray photoelectron spectroscopy (XPS, PHI 5000 VersaProbe, Ulvac-PHI, Japan) to detect the chemical composition of the fabricated scaffolds with or without surface modification (n = 3/per group) at a base pressure inside the analyzer of $2 \times 10^{-7}$ Pa. The photoelectron spectra were excited using a monochromated Al Kα (1486.6 eV) anode at a constant power of 25 W (15 kV and 10 mA). During spectra acquisition, the constant analyzer energy mode had a narrow scan pass energy of 58.70 eV and pass energy with a 0.1 eV step. The binding energy scale was calibrated for hydrocarbon contamination using the C1s peak at 285 eV.

### 2.3. Mechanical properties of the MDP and MDP-DOPA scaffolds

Tensile strength was evaluated according to the ASTM D882 standard method using a tensile test machine (Model 5966, Instron, MA, USA). The size of the samples was prepared to 1.5 cm × 3 cm. The MDP and MDP-DOPA scaffolds (n = 5/per group, hydration state) were tested at a load cell force of 10 kN, a crosshead speed of 10 mm/min, and a clamp distance of 25 mm. The MDP and MDP-DOPA scaffolds were clamped between two holders. Also, MDP and MDP-DOPA scaffolds (n = 5/per group, hydration state) were compressed at a rate of 0.15 mm/s until mechanical failure. Mechanical test results including tensile stress, tensile strain, Young's modulus and compressive stress were output via the manufacturer's program.

### 2.4. Mass spectrometry analysis

Casein protein component reduction was performed using 10 mM dithiothreitol (DTT) in the dark for 1 h, and alkylation was achieved afterward with 30 mM 2-chloroacetamide in the dark for 1 h. The reaction was quenched by the addition of 20 μL of 200 mM DTT and incubation for 10 min. The samples (n = 3/per group) were diluted (1:10 casein:ammonium hydrogen carbonate (v/v)) using 25 mM ammonium bicarbonate, and the diluted samples were treated with 2 μg of sequencing-grade trypsin (Promega) at 37 °C for 12 h followed by the addition of trypsin to the reaction mixture for an additional 6 h. Finally, the samples were desalted using a C18 solid-phase extraction pipette tip (SPEC PT C18, Varian), vacuum-dried, and then dissolved in 10 μL of 95% $H_2O$, 5% acetonitrile, and 0.1% formic acid for subsequent mass spectrometry (MS) analysis.

The MS analyses were conducted with a high-performance liquid chromatograph (Waters nanoAcquity) combined with an electrospray ionization (ESI) FT/ion-trap mass spectrometer (LTQ Orbitrap Velos, Thermo Fisher Scientific). Peptides were separated using a 50 × 365 μm fused silica capillary micro-column packed with 15 cm of 5 μm diameter C18 beads (Western Analytical Products) followed by a 5 cm trap column (75 × 365 μm, 5 μm-diameter C18 beads). The peptides were eluted at a 0.2 μm/min flow rate using a linear gradient from 5% to 50% acetonitrile in 0.1% formic acid. A full-range mass spectral scan was achieved in the orbitrap, and the acquired raw MS/MS spectra files for each sample were analyzed against the bovine and mammalian protein UniProt database using SEQUEST (version 1.2, Thermo Fisher

Scientific).

### 2.5. In vitro degradation test

The in vitro degradation of the MDP and MDP-DOPA scaffolds (n = 5/per group) was investigated by incubating each sample in a 1 mg/mL collagenase B (Roche, Basel, Switzerland) solution, which induced enzymatic degradation to indirectly predict implanted scaffold behaviors in vivo and measured the weight loss over 28 days [18,19]. To mimic host physiological condition, collagenase B was further dissolved in bovine serum collected from whole bovine blood (Farm Story Hannaeng, Cheongju, Korea) by centrifugation (3000 rpm) and the prepared samples were incubated at 37 °C. Each scaffold was weighed at each time point (1, 7, 14, and 28 days) after washing with DW three times and dried to remove excess solvent. At every time point (t), the weight loss was calculated according to the following formula: weight loss (%) = (Wi - Wt)/Wi x 100, where Wi represents the initial weight and Wt represents the weight of the sample at the indicated time point.

### 2.6. In vitro cytotoxicity and proliferation tests

The cytotoxicity of MDP and MDP-DOPA scaffolds to rat bmMSCs (Lonza, USA) and mouse RAW 264.7 cells (American Type Culture Collection, Bethesda, MD, USA) was evaluated using the LIVE/DEAD™ viability/cytotoxicity kit (Invitrogen) according to the manufacturer's protocols. The bmMSCs and RAW 264.7 cells were cultured with a growth medium, which was Dulbecco's modified Eagle's medium (DMEM, Corning, USA) supplemented with 10% fetal bovine serum (FBS, Corning) and 1% penicillin/streptomycin (PS, Corning) until they were confluent. The bmMSCs and RAW 264.7 cells (each $5 \times 10^4$ cells/mL) were cultured on scaffolds (n = 5/per group) for 5 days in 24 well culture plates and the resulting samples were washed twice with sterile phosphate-buffered saline (PBS, Sigma-Aldrich). The LIVE/DEAD reagents (4 μM EthD-1 and 2 μM calcein-AM) were added directly to the samples, which were then incubated for 30 min at 37 °C and finally, observed using a fluorescence microscope (IX71 inverted microscope, Olympus, Tokyo, Japan) at the Center for Bio-medical Engineering Core Facility (Dankook University, Cheonan, Korea). We quantified the green labeled cells to analyze cell viability ([green labeled cells/total number of cells] × 100) using Image J software (National Institutes of Health, Bethesda, MD, USA). Cell proliferation was examined using the Cell Counting Kit-8 (CCK-8, Dojindo, Japan). At each time point (1, 3, and 5 days), the cultured bmMSCs and RAW 264.7 cells (each $5 \times 10^3$ cells/mL) on the scaffolds (n = 5/per group) in 96-well culture plates were washed twice using PBS, and 10 μL of CCK-8 solution in 100 μL of growth media was added to each well of the culture plate. The culture plates were incubated at 37 °C for 3 h and the absorbance was measured at 450 nm using a microplate reader (Spark 20 M multimode microplate reader, Tecan, Männedorf, Switzerland). We quantified the cell proliferation rate using the following equation: viable cells (%) = [(absorbance value of each group)/(absorbance value of control group (tissue culture plates))] × 100.

### 2.7. In vitro β-casein release test

To investigate protein release kinetics, 6 mg of MDP and MDP-DOPA scaffolds (n = 5/per group) were placed in 1.5 mL standard polypropylene microtubes and immersed in 1 mL of 1% bovine serum albumin (BSA)-PBS solution at 37 °C. At each time point, the solution was removed from each tube and replaced with fresh BSA-PBS. The selected sampling time points were 1, 3, 5, 7, 14, and 28 days. The collected samples were analyzed using an enzyme-linked immunosorbent assay kit for beta-casein (ELISA kit for casein beta, SEJ332Bo, Cloud-Clone Corp., TX, USA) according to the manufacturer's protocol.

### 2.8. In vitro cell migration assay

To investigate improvements in migratory performance by our materials, MDP and MDP-DOPA scaffolds (n = 5/per group) with or without RAW 264.7 cells ($5 \times 10^4$ cells/mL) were placed in 24 well plates before cell seeding onto transwell inserts (Corning). The bmMSCs ($1 \times 10^5$ cells/mL) and RAW 264.7 cells ($1 \times 10^4$ cells/mL) were seeded onto transwell inserts with a polycarbonate membrane pore size of 8 μm (bmMSCs) and 5 μm (RAW 264.7 cells) (Corning) in 24 well plates. After 1 day, the growth medium was removed and the transwell inserts were fixed with 4% paraformaldehyde (Sigma-Aldrich) for 1 min. The non-migrated cells on the upper layer of the transwell insert membranes were gently removed using a cotton swab. The migrated cells on the bottom layer of the transwell inserts were stained with 0.05% crystal violet (Sigma-Aldrich) for 10 min and observed using a microscope (AZ100, Nikon, Japan). For colorimetric quantification, the stained cells were immersed in 10% acetic acid and incubated for 30 s. The lysed solutions were measured at an optical density of 590 nm using a microplate reader.

### 2.9. Collection of RAW 264.7 conditioned media and M1/M2 polarization

Macrophage polarization was investigated using RAW 264.7 cells. RAW 264.7 cells ($5 \times 10^6$ cells/scaffold) were seeded in 100 mm diameter MDP and MDP-DOPA scaffolds with growth medium for 24 h. CM collected from treated RAW 264.7 cells was centrifuged for 20 min at 300 g to remove any residual substance. The RAW 264.7 cells cultured on the scaffolds (n = 5/per group) were detached from each scaffold and M1/M2-related gene expression was evaluated. We isolated RNA from the cells using an RNA extraction kit (Accuprep Universal RNA Extraction Kit, Bioneer) according to the manufacturer's protocol. RNA was quantified by absorbance readings at 260 nm and 280 nm using a Nanodrop spectrophotometer (Thermo Fisher Scientific). The RNA was purified, and first-strand cDNA was synthesized from 1 μg of total RNA using RT-PCR premix (Bioneer). The synthesized cDNA was used as a template for the amplification of each M1/M2 marker in PCR reactions containing PCR premix (Bioneer) and primers (Tables S3 and S4). The RT-PCR products were resolved by agarose gel electrophoresis.

### 2.10. In vitro osteogenic differentiation test

To investigate the relationship between macrophages and bmMSC osteogenic differentiation, the CM collected from RAW 264.7 cells was mixed with osteogenic differentiation media (100 nM dexamethasone, 50 mM L-ascorbic acid, 10 mM β-glycerophosphate, and 7 mM L-glutamine in growth medium) in the same volume ratio. BmMSCs ($5 \times 10^4$ cells/mL) were seeded in 15 mm diameter MDP and MDP-DOPA scaffolds (n = 5/per group, each experiment) with CM. The bmMSCs were cultured, and fresh medium was added every 2 days for 1, 2 and 4 weeks. After each time point, osteogenic differentiation was evaluated using various methods. First, bmMSCs were detached from each scaffold and used for measuring osteogenic differentiation-related gene expression by RT-PCR analysis using the same method described above. Moreover, osteogenic differentiation-related protein levels were analyzed by immunocytochemistry. The bmMSCs were fixed with 4% paraformaldehyde for 15 min and washed 3 times with PBS. The washed cells were blocked for 1 h with 5% goat serum and 0.1% Triton X-100 in PBS at room temperature. The blocked cells were stained with primary antibody (ALP: sc-271,431, OPN: ab8448) overnight at 4 °C. Then, fluorescein-isothiocyanate-conjugated secondary antibodies (Jackson Immuno Research Laboratories) were used to visualize with positive primary antibody signals and counterstained with 4′,6-diamidino-2-phenylindole (DAPI-Vectashield, Vector Laboratories, Burlingame, CA, USA). The immunostained cells were photographed using fluorescence microscopy. Image J software was used to analyze the positive signals in

the images. In addition, ALP-extracted IGEPAL solution (Sigma-Aldrich) and p-nitrophenyl phosphate solution were added to a 96-well plate and incubated at 37 °C for 30 min. After 30 min, 0.5 N NaOH (Sigma-Aldrich) was added to stop the color reaction, which was read with a plate reader at 410 nm. ALP activity was normalized to DNA content, which was detected using a PicoGreen dsDNA quantitation kit (Sigma-Aldrich). The calcium content was measured using a calcium colorimetric assay kit (Sigma-Aldrich). The osteogenically differentiated cells on both MDP and MDP-DOPA scaffolds were decalcified with 300 μL of 0.6 N HCl for 24 h at room temperature. The extracted calcium solution was used for calcium quantification according to the manufacturer's protocols and detected at 575 nm using a plate reader.

### 2.11. In vivo animal test

Female ICR mice (six weeks old, Dayun, Gyeonggi-do, Korea) were prepared and anesthetized by the intraperitoneal injection of a ketamine and xylazine mixture (4:1 ratio). After sterilizing the mouse's head, a longitudinal incision was performed on the midline of the cranium to expose the sagittal suture line. We prepared two circular transosseous defects of 4 mm on the skull using a surgical trephine burr (XTP3404, Dentium, Seoul, Korea). The defect site was frequently cooled with sterile saline to prevent additional tissue damage. We conducted 3 different studies to evaluate host cell migration, new bone formation, and mineral deposition by the recruited host cells, as well as cytokine absorption. The prepared MDP and MDP-DOPA scaffolds were implanted into mouse subcutaneous tissue (n = 4 per group) and the calvaria defect sites (n = 10 per group) for new bone formation. After 1 week, the implanted samples were retrieved from the subcutaneous tissue for further analysis related to host cell migration. To investigate mineral deposition by the cells recruited to each implanted scaffold, the implanted scaffolds were retrieved from mouse calvaria after treatment for 1 and 2 weeks, and the implanted scaffolds were transplanted between the subcutaneous tissue and muscle tissue in mice hindlimbs for 2 different durations. Also, to verify the types of recruited macrophages, the cytokines secreted in the defect area in the early stage were analyzed, and we retrieved the implanted scaffolds at 3 days and 1 week for investigations. After 2 and 4 weeks in the mouse hindlimb and 3 days, 1 week, and 8 weeks in the mouse subcutaneous and calvarial defect model, all mice were euthanized by $CO_2$ asphyxiation. The retrieved samples and harvested skull bones were fixed in 4% PFA overnight. The animal study was approved by the Institutional Animal Care and Use Committee at Dankook University (DKU-20-022).

### 2.12. Live micro-CT analysis

At each time point (2, 4, and 8 weeks), the MDP and MDP-DOPA scaffold-implanted mice were anesthetized by intraperitoneal injection in the same manner as that used for animal surgery. The anesthetized mice were analyzed using micro-CT scans (Skyscan 1176, Skyscan, Kontich, Belgium). Micro-CT was conducted at 50 kV and 500 μA, with a 0.2-mm aluminum filter, and scanning was performed on all specimens (n = 10/per group). The scanned images were reconstructed using the Skyscan NRecon program. Following reconstruction, regions of interest were determined in the images for the Skyscan CTan and CTvol for visualizing and quantifying the newly formed bone volume (BV/TV) and mineral density (BMD).

### 2.13. Histological analysis

After 2, 4, and 8 weeks, all mice were euthanized and mice hindlimb muscles including scaffolds and skulls were harvested and fixed in 4% PFA overnight for further histological analysis. The fixed specimens (n = 10/per group) were washed in PBS to removed residual PFA and immersed in decalcifying Solution-Lite (Sigma-Aldrich) at room temperature for 2 h. Then, the samples were dehydrated in a graded ethanol series and xylene and embedded in paraffin. The embedded samples were sectioned into 6 μm sizes using a microtome (RM2255, Leica, Bensheim, Germany) and deparaffinized in xylene, hydrated in a graded ethanol series, stained with hematoxylin/eosin (H&E, Sigma-Aldrich), Goldner's trichrome (BIOGNOST®, Zagreb, Croatia), and Von Kossa (Abcam) stain. The stained samples were photographed using an optical microscope to investigate the bone formation area and bone density. The bone formation area and bone density were measured using the following equation: new bone formation area = [(newly formed bone area)/(original defect area)] × 100; bone density = [newly formed bone area/(newly formed bone area + fibrovascular tissue area)] × 100.

### 2.14. Immunohistochemical analysis

To confirm the expression level of osteocalcin (OCN, 1:100, Abcam), F4/80 (1:20, R&D Systems), CD44 (1:100, Novus Biologicals), ALP (1:200, Santa Cruz), CD86 (1:200, Novus Biologicals) and CD206 (1:20, R&D Systems), we randomly selected paraffin-sectioned slides (n = 10/per group) at each time point and immersed them in xylene for deparaffinization. Then, the samples were hydrated in an immunostaining preconditioning process and incubated using a blocking buffer solution containing 10% horse serum and 0.5% Triton X-100 in PBS at room temperature. The blocked samples were stained with primary rat-specific antibodies overnight at 4 °C. We used fluorescein-isothiocyanate-conjugated secondary antibodies (Jackson Immuno Research Laboratories) to visualize the positive signals of the primary antibodies and counterstained the samples with DAPI. The immunostained samples were photographed using a fluorescence microscope (IX71 inverted microscope, Olympus, Tokyo, Japan). To compare positive expressions of CD86 and CD206 between analysis groups, we evaluated photographed images to use Image J software.

### 2.15. Secreted cytokine array analysis in the early stage after implantation

After 1 week, the samples (n = 5/per group) harvested from mouse calvaria were homogenized in PBS with protease inhibitor (10 μg/mL of pepstatin, aprotinin, leupeptin), and Triton X-100 was added to a final concentration of 1% and frozen at ≤ −70 °C, thawed, and centrifuge at 10,000 g for 5 min and the supernatant was collected. The supernatants were assayed using the Proteome Profiler Array Mouse XL Cytokine Array Kit (ARY028, R&D Systems) according to the manufacturer's protocol. The array kit contains nitrocellulose membranes spotted with capture antibodies. Each membrane was incubated with supernatant at 4 °C overnight. After extensive washing to remove non-bound proteins, the membranes were incubated with biotinylated detection antibodies. Next, streptavidin–horseradish peroxidase was added to visualize the antibody reactions, which were detected using an image analyzer system (ImageQuant LAS 4000 mini, GE Healthcare).

### 2.16. Statistical analysis

The quantitative data are expressed as the mean ± standard deviation. We used Origin Pro 8 SR4 software (OriginLab Corporation, MA, USA) to perform the Student's t-test. A P-value of $<0.05$ was considered to denote statistical significance.

## 3. Results and discussion

### 3.1. Characterization of milk-derived protein scaffolds

MDP and MDP-DOPA scaffolds were fabricated with a combination of casein and PVA solutions through freeze-thaw cycles to improve the mechanical properties and degradation rate (Fig. 1A) [20]. The repeated freeze-thaw cycles induced physical cross-links between casein and PVA by physical sol-gel transition without any crosslinking agent [21]. The

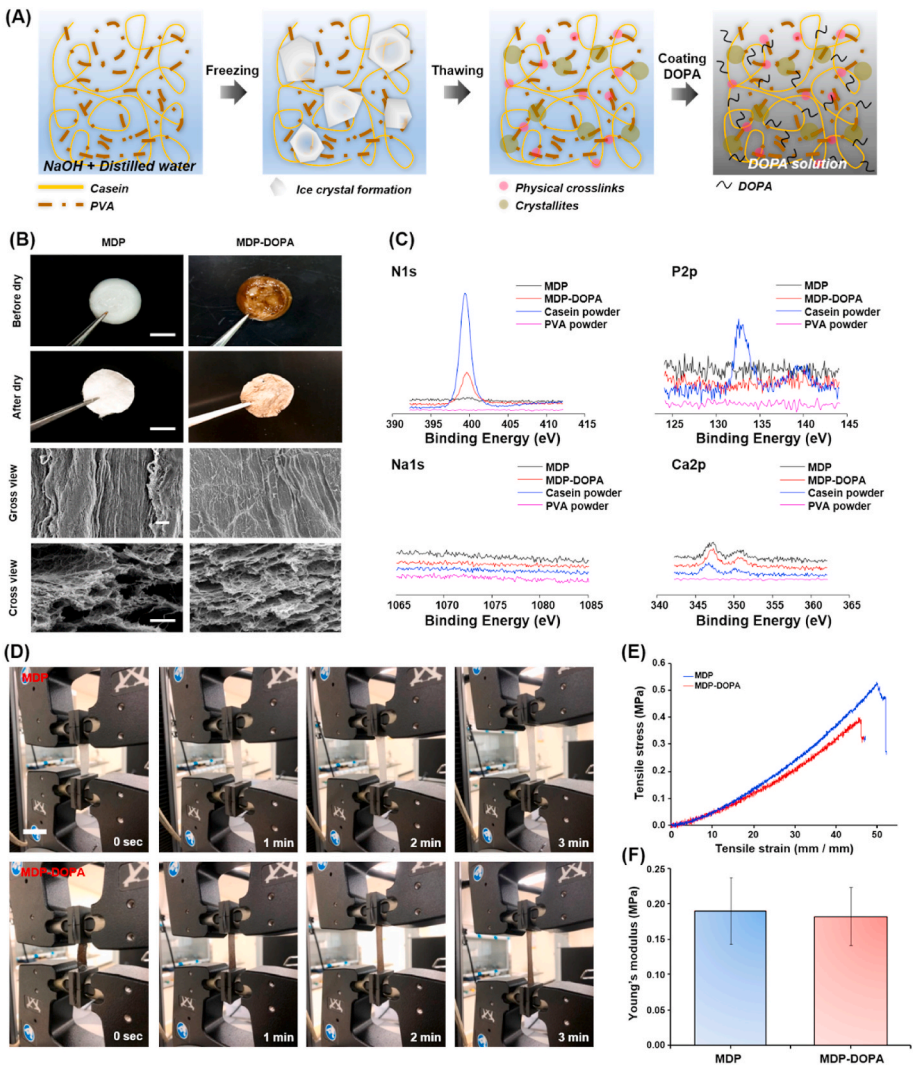


**Fig. 1.** (A) The fabrication procedure of MDP and MDP-DOPA scaffolds. (B) Morphological characterization of MDP and MDP-DOPA scaffolds using SEM (n = 3/per group, Macroscopic images scale bar = 5 mm, SEM image scale bar = 100 μm). (C) Surface characterization using XPS analysis of various materials (n = 3/per group). (D) The evaluation of mechanical property of MDP and MDP-DOPA scaffolds (n = 5/per group, Scale bar = 25 mm). The quantification results of (E) tensile strain-stress curve and (E) Young's modulus.

MDP was coated with DOPA to promote better adhesion of the host cells or cytokines onto the surface of the scaffold. DOPA enhances the absorption of cell-binding proteins via the reactivity of amine and thiol groups [22]. During the coating of DOPA onto the MDP scaffold, DOPA polymerization occurred homogeneously over the entire surface of the MDP scaffold and the color gradually changed to dark-brown (Fig. 1B). The MDP and MDP-DOPA scaffolds showed sponge-type shape and similar structure except for their color in macroscopic images before or after freeze-drying. In a detailed structure investigation, we conducted a morphological analysis of freeze-dried MDP scaffolds using scanning electron microscopy (SEM). In the gross view, the surface of the MDP and MDP-DOPA scaffolds had a somewhat flat surface and inner uniaxial structures were seen on the cross-sectional view. PVA fibrillation resulted in the phase transformation of the MDP and MDP-DOPA scaffolds from semi-crystalline to amorphous structures during fabrication. Water molecules penetrated the molecular chains of PVA and were weakly bound to the hydroxyl groups [23]. This process caused the re-arrangement or reorientation of PVA molecules in the MDP scaffold. We also confirmed that DOPA coating did not deform surface morphology. The cross-sectional view in both groups showed porous structures which were occupied and formed by ice crystals that composed the layered structure.

Surface analysis was performed by X-ray photoelectron spectroscopy (XPS) to detect the chemical composition of the fabricated scaffolds with or without surface modification, as shown in Fig. 1C. PVA powder group was not detected any peaks in narrow scans at nitrogen (N1s, 399.73 eV), phosphorus (P2p, 133.17 eV), sodium (Na1s, 1071.7 eV) or calcium (Ca2p, 347.02 eV) [24]. The casein powder group showed higher counts of N1s, P2p peaks compared to the other groups [25–27]. The counts levels of Ca2p peaks were analyzed comparable with Casein powder, MDP and MDP-DOPA groups. The MDP-DOPA group had higher N1s peaks than the MDP group because the catecholamine groups in DOPA were covered in the MDP group and exposed on the surface of the MDP-DOPA group [28]. Both the MDP and MDP-DOPA groups had similar levels in P2p peaks. The phosphoric acid in the chemical structure of casein was considered to be surrounded by the PVA chains re-arranged during the MDP fabrication process. Thus, it was not detected in either the MDP or the MDP-DOPA group. Furthermore, mass spectrometric analysis of MDP and MDP-DOPA scaffolds was performed to identify the biochemical composition of scaffolds and preserve milk protein from physical cross-links. We confirmed that MDP and MDP-DOPA scaffolds retained α-, β- and κ-caseins including other types of proteins (Tables S1 and S2).

We also examined and calculated mechanical property values including tensile stress, Young's modulus and compressive stress in the MDP and MDP-DOPA groups by Instron (Fig. 1D to F). The tensile stress-strain curves appeared to have similar yield strengths in both the MDP and MDP-DOPA groups. Young's modulus in the MDP (0.19 ± 0.05 MPa) and MDP-DOPA (0.18 ± 0.04 MPa) groups also had comparable values without significant differences. Compressive modulus was

investigated, with no significant difference between the MDP (5.55 ± 0.41 kPa) and MDP-DOPA (5.34 ± 0.64 kPa) groups (Fig. S1). As we confirmed to compare surface morphologies using SEM between MDP and MDP-DOPA groups, DOPA coating was not affected mechanical properties. For effective bone regeneration in the bone defect area, the implanted materials should maintain mechanical support during the regeneration process [29]. Thus, we performed an in vitro degradation test for 4 weeks (Fig. S2) and found that the degradation rates in the MDP (6.29 ± 2.37%) and MDP-DOPA (6.27 ± 1.96%) groups showed similar tendencies. Based on those data, we considered both the MDP and MDP-DOPA scaffolds to be suitable for applications in vitro and in vivo studies on bone regeneration.

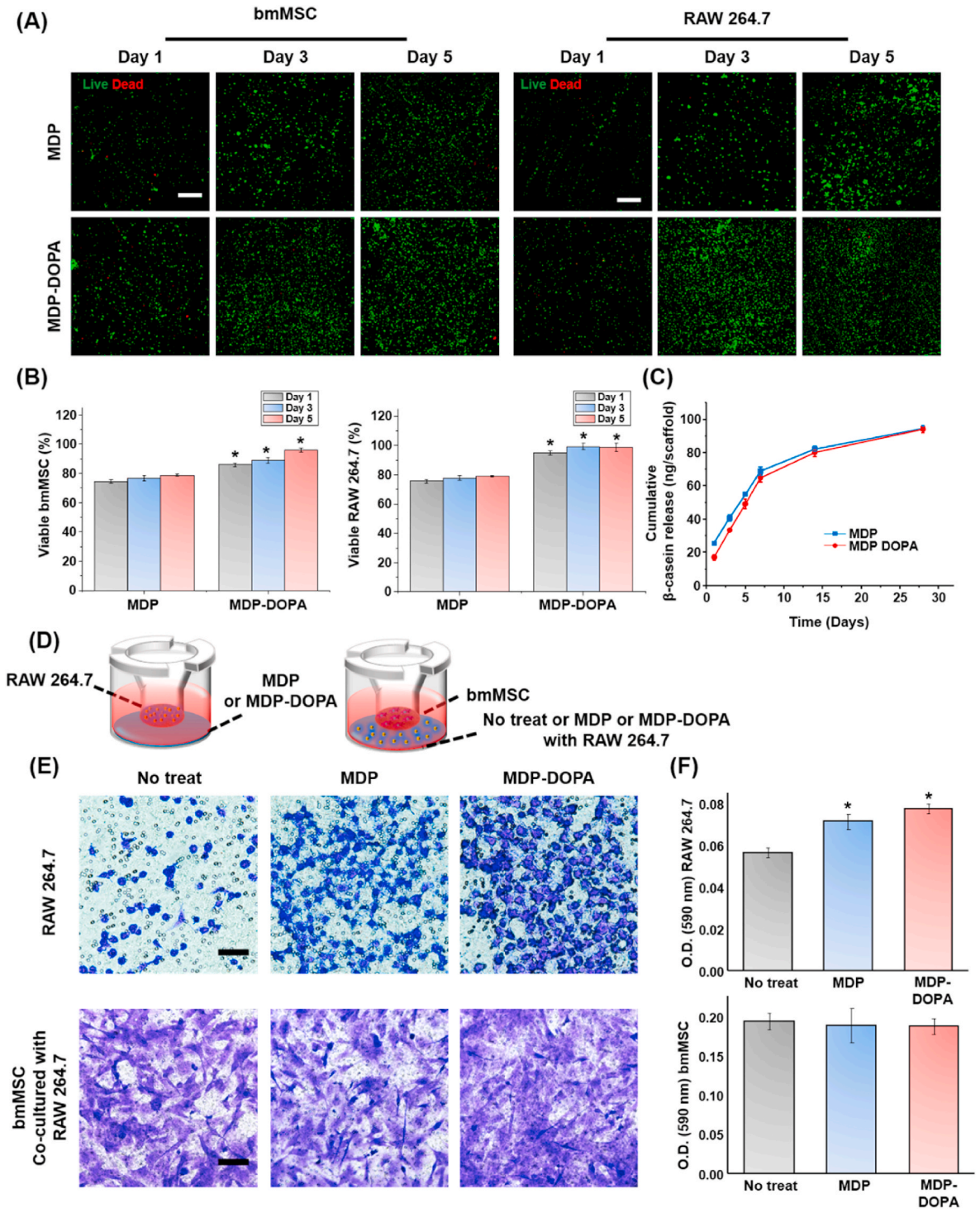


**Fig. 2.** In vitro cytotoxicity and cell proliferation tests were performed to use MDP and MDP-DOPA scaffolds. (A) Live & Dead and (B) CCK-8 assays of bmMSC and RAW 264.7 cells in scaffolds (n = 5/per group, $p^* < 0.05$ compared with MDP, Scale bar = 1 mm). (C) The quantification results of cumulative β casein release test from MDP and MDP-DOPA scaffolds (n = 5/per group). (D) The schematic illustration of indirect RAW 264.7 and bmMSC migration tests using transwell-inserts. (E) Representative images of RAW 264.7 and bmMSC migration tests (n = 5/per group, Scale bar = 50 μm). (F) The quantification results of RAW 264.7 and bmMSC migration rate ($p^* < 0.05$ compared with No treat).

### 3.2. In vitro cytotoxicity and migration tests

To examine the cytotoxicity and cell viability of bone marrow mesenchymal stem cells (bmMSCs) and RAW 264.7 cells on the MDP and MDP-DOPA scaffolds, LIVE/DEAD and CCK-8 assays were performed (Fig. 2A and B). We compared the green color (live cells) and red color (dead cells) of the bmMSCs and RAW 264.7 cells on the MDP and MDP-DOPA scaffolds at each time point. Both cell types mostly expressed green signals with a few red dots in all groups at all time points. The quantification results and numerical values of the LIVE/DEAD assay were added to Fig. S3. However, the MDP group showed much lower cell densities compared to the MDP-DOPA group at each time point. In the same manner, the CCK-8 assay results showed significantly lower cell population MDP group than MDP-DOPA groups at each time point. These results were not considered to be related to cytotoxicity, but because of the many hydrophobic domains in casein [12] and hydrophilic PVA [30], the bmMSCs and RAW 264.7 cells did not easily attach to the surface of the scaffold. We also confirmed that bmMSCs on the MDP scaffold did not appear to spread at 36 h compared to the MDP-DOPA scaffolds and affected initial cell adhesion through F-actin with vinculin staining and SEM images (Fig. S4). Thus, to improve the initial cell adhesion, we coated the surface of MDP with DOPA. The DOPA grafted onto the MDP scaffold had an abundance of functional amine groups with positive charges and these would interact electrostatically with negatively charged glycoproteins in the cell membranes [31]. Thus, better cell proliferation could be induced by enhanced cell adhesion.

We also analyzed the accumulated release profiles of substances such as β-casein from the prepared MDP and MDP-DOPA scaffolds (Fig. 2C). We conducted release tests of β-casein from both the MDP and MDP-DOPA scaffolds over 28 days. The cumulative β-casein release after 28 days was not significantly different between the MDP (94.47 ± 1.45 ng) and MDP-DOPA (94.12 ± 2.10 ng) scaffolds. β-casochemotide-1 in β-casein was previously reported to induce high levels of macrophage chemotaxis [15]. Macrophages have been reported to play an essential role in sustaining bone homeostasis and defect healing by inducing the recruitment and differentiation of mesenchymal progenitor cells [32]. To investigate these concepts in the present research, we performed 1 day in vitro transwell cell migration tests of both RAW 264.7 cells and bmMSCs (Fig. 2D to F). First, we evaluated the migratory performance of RAW 264.7 cells toward MDP and MDP-DOPA scaffolds, which released β-casein for recruiting RAW 264.7 cells toward the materials. Compared to the no-treatment (0.06 ± 0.01) group, both the MDP (0.07 ± 0.01) and MDP-DOPA (0.08 ± 0.01) groups showed significantly higher RAW 264.7 migration rates. Furthermore, we implanted both MDP and MDP-DOPA scaffolds into mouse subcutaneous tissue for 1 week to investigate the recruitment of host macrophages (Fig. S5). The MDP and MDP-DOPA groups showed significantly higher deposition of F4/80, CD86 and CD206-positive cells around the implanted area compared to that of the polycaprolactone (PCL) and PCL-DOPA films used as the control groups. Second, we performed cell migration tests to the MDP and MDP-DOPA scaffolds with RAW 264.7 cells, which were placed on the bottom of the culture plate well and bmMSCs that were seeded on the transwell insert. The bmMSC migration rate was not significantly different between the no-treatment (0.19 ± 0.01), MDP (0.19 ± 0.02), and MDP-DOPA (0.19 ± 0.01) groups, suggesting that the chemokines secreted from the macrophages induced equivalent chemotaxis in each group and directly affected bmMSC migration to similar levels regardless of whether MDP or MDP-DOPA scaffolds were used [33]. The in vitro and in vivo analyses indicated that β-casochemotide-1 in the β-casein in our MDP and MDP-DOPA scaffolds could recruit macrophages.

### 3.3. In vitro osteogenic differentiation tests

The understanding of macrophage behavior at the areas of implanted biomaterials is very important because such materials can induce potential inflammatory responses, which determine the shift to the next healing stage [34]. When a bone fracture occurs, inflammation is initiated, including the release of inflammatory cytokines for macrophage polarization to the M1 phenotype, which plays a crucial role in phagocytic and clearance processes [35]. Following this process, the anti-inflammatory phase involves M2 phenotype macrophages, which contribute to the synthesis of the extracellular membrane (ECM) and vessel formation. In the present study, the tissue regeneration process from the recruitment of many macrophages by β-casochemotide-1 in casein in the early stage might be enhanced or prolonged. If the pro-inflammatory response is prolonged for certain reasons such as excessive immune reactions, tissue regeneration is delayed by hindering M1 and M2 phase transition [35]. Thus, inducing tissue regeneration modulated by the interaction between implanted biomaterials and host cells during the pro-inflammatory response has a huge benefit. As the macrophages recruited and attached to implants can sense the surface of the implants, certain macrophage phenotypes are activated, which secrete specific cytokines that are able to induce a series of healing processes [34]. Therefore, we investigated whether seeding RAW 264.7 cells on MDP and MDP-DOPA scaffolds could induce certain macrophage polarization. First, RAW 264.7 cells were seeded on both MDP and MDP-DOPA scaffolds, which were cultured for 1 day (Fig. 3A). Then, the expression of already reported M1 and M2 macrophage-related genes was analyzed in RAW 264.7 cells cultured on MDP or MDP-DOPA (Fig. 3B and C) [36]. Real-time polymerase chain reaction (PCR) analysis showed that the MDP group had an increased expression of M1-associated genes including CD86, TNFα, CCL19, and CXCL11, whereas the MDP-DOPA group showed the enhanced expression of M2-associated genes, CD163, CD206, IL-10, and CCL13 without any external stimulation. Specifically, the MDP-DOPA group also showed a high expression of the BMP-2 gene compared to the MDP group. These results indicated that the RAW 264.7 cell phenotype was not completely changed, but MDP-DOPA scaffolds strongly induced the specific polarization of RAW 264.7 cells to the M2 lineage. In the case of the MDP scaffold, it was hard to induce the polarization of M2-like macrophages because the PVA in the MDP scaffold had robust hydrophilic properties that caused the reversible adsorption of proteins [37]. It was barely induced to form cell binding proteins by seeded cells on MDP scaffold. However, the MDP-DOPA group was prepared with a surface modification to improve binding cells, proteins and various cytokines. The cell-binding proteins were easily attached to the surface of the scaffold and interaction between integrin β1 in RAW 264.7 cells and cell-binding proteins might induce M2 polarization [38]. To exclude to possible influences of casein and DOPA in the polarization of RAW 264.7 cells, we used TCPS, PCL, and PCL-DOPA films in the same manner as in Fig. 3B and C (Fig. S6). We confirmed that the TCPS, PCL, and PCL-DOPA groups did not show significant differences in gene expression in specific immune cells. We proved that DOPA did not contribute to RAW 264.7 cell polarization.

Second, to examine the influence of CPP and cytokines secreted from cultured RAW 264.7 cells on different scaffolds on the osteogenic differentiation rate, we performed in vitro osteogenic differentiation tests. Only the PVA group was exclused from the in vitro osteogenic differentiation tests because various in vitro and in vivo studies reported the inadequate osteogenic performance of PVA [39–41]. Before culturing bmMSCs with MDP or MDP-DOPA scaffolds, we collected conditioned media (CM) from RAW 264.7 cells cultured on each scaffold for 1 day (Fig. 3D). After 1 week, bmMSCs cultured on the MDP-DOPA scaffold showed the high

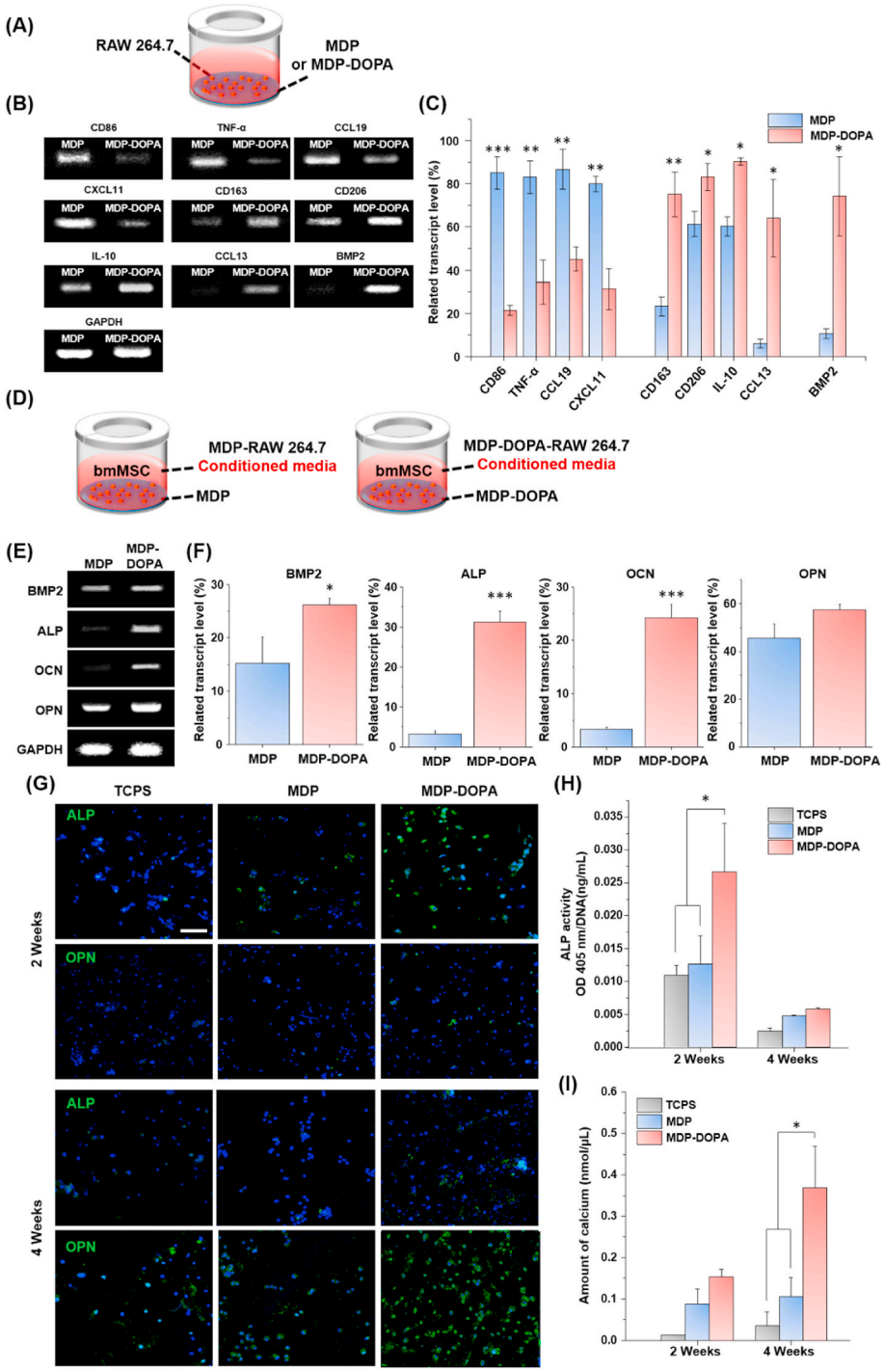


**Fig. 3.** (A) Schematic illustration of inducing M1/M2 polarization on MDP and MDP-DOPA scaffolds. (B) M1 and M2 related gene expression profiling of RAW 264.7 cells through RT-PCR after culture at 24 h and (C) its quantification results (n = 5/per group). (D) Schematic illustrations of in vitro osteogenic differentiation test of bmMSC using RAW 264.7 conditioned media. (E) Osteogenic related gene expression profiling of bmMSC using RT-PCR and (F) quantification results of band pixel density at 1 week (n = 5/per group). (G) The evaluation of ALP and OPN positive signal of bmMSC on MDP and MDP-DOPA scaffolds through immunocytochemical analysis for 2 and 4 weeks (n = 5/per group, each experiment, Scale bar = 200 μm). The quantification results of (H) ALP activity and (I) calcium contents of bmMSC on MDP and MDP-DOPA scaffolds for 2 and 4 weeks (n = 5/per group, each experiment, $p^* < 0.05$, $p^{**} < 0.01$, and $p^{***} < 0.001$).

mRNA expression of osteogenic-related genes such as BMP-2, alkaline phosphatase (ALP), osteocalcin (OCN), and osteopontin (OPN) compared to the MDP scaffold (Fig. 3E and F). The MDP-DOPA scaffold also showed the high expression of ALP-positive signals and quantification results in bmMSCs in 2 weeks compared to the controls and MDP scaffold (Fig. 3G and H). Furthermore, the MDP-DOPA scaffold showed a higher expression of OPN-positive signals and calcium deposition in bmMSCs in 4 weeks than in the other groups (Fig. 3I). The detailed quantification results and the numerical ALP and OPN positive expression values were added to Fig. S7. The bmMSCs with MDP-DOPA scaffolds showed higher expressions of early and later osteogenic-related markers, suggesting that the MDP-DOPA scaffold CM contained abundant BMP-2. In addition, CPP, which is distributed through various casein fractions, was contained in the MDP-DOPA scaffold and its calcium-binding properties have been reported to consist of three phosphoserines and two glutamic acids [13]. This negatively charged region was exposed on the surface and facilitated the formation of bonds with $Ca^{2+}$ ions [14]. Previous research demonstrated that CPP behavior had a crucial role in osteogenic differentiation such as modulating bone-forming cell activity and mineral deposition in vitro and/or in vivo [42].

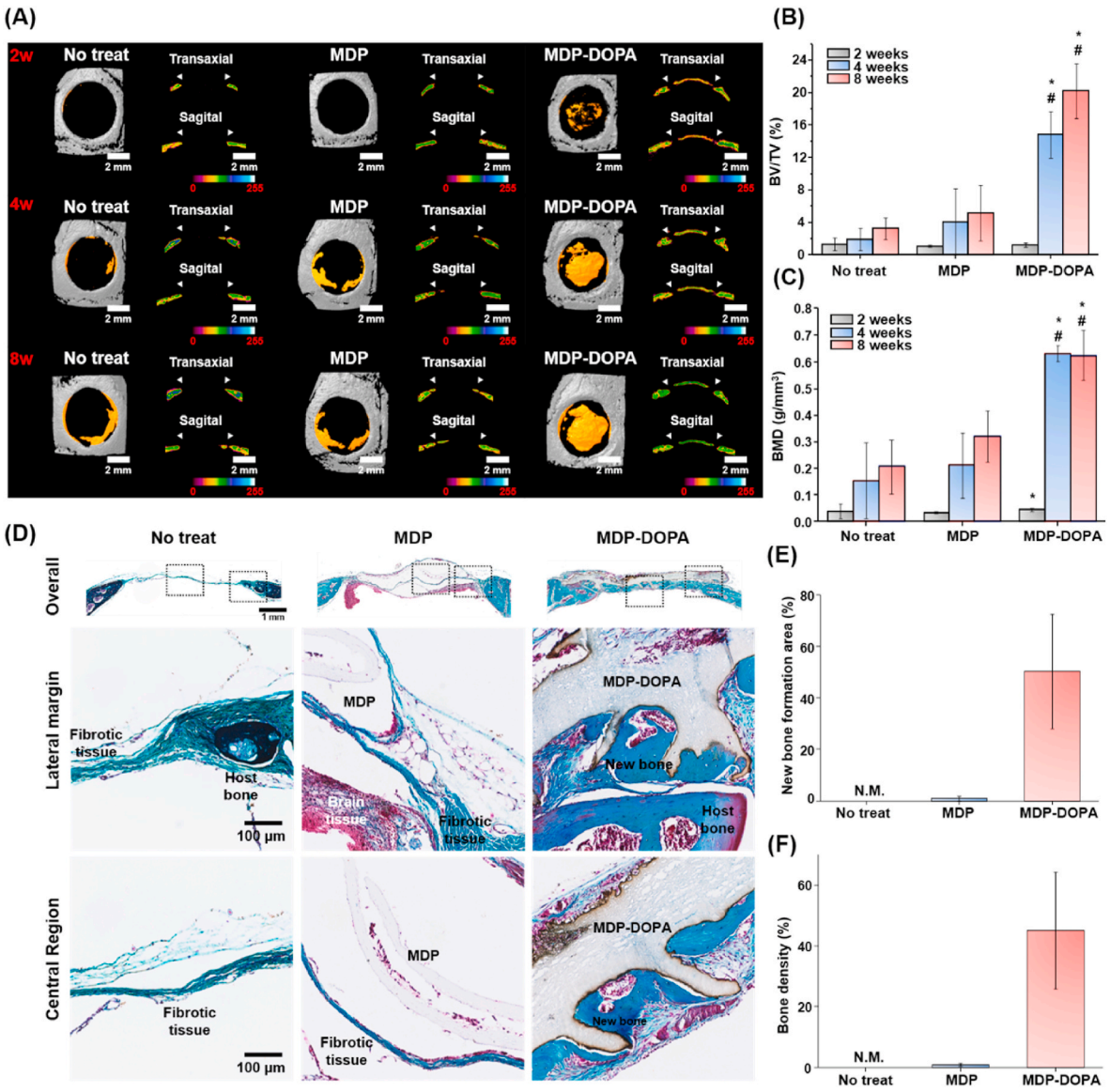


**Fig. 4.** In vivo mouse calvarial defect models were performed using MDP and MDP-DOPA scaffolds. (A) Live micro-CT analysis was progressed to examine rate of mineral deposition at defect site for 2, 4 and 8 weeks (n = 10/per group, each time point). White arrowheads indicated the margin of defect. At each time points, (B) BV/TV and (C) BMD of MDP and MDP-DOPA groups were measured. (D) After 8 weeks, histological analysis was performed to use Goldner's trichrome staining (n = 10/per group). Black dotted square boxes indicated the images that were magnified to margin and center area. The quantification results of (E) new bone formation area and (F) bone density at defect area (p* < 0.05 compared with No treat, p# < 0.05 compared with MDP).

### *3.4. In vivo orthotopic bone formation in the mouse calvarial defect model*

We implanted MDP and MDP-DOPA scaffolds into the mouse calvarial defect model to conduct a more detailed analysis of the efficacy of new bone formation (Fig. 4A to C). We analyzed the newly formed bone volume per tissue volume (BV/TV) and bone mineral density (BMD) at each time point (2, 4, and 8 weeks) using live micro-computed tomography (CT). Representative three-dimensional (3D) and soft X-ray images of mineralized new bone formation by micro-CT are shown. At 2 weeks, the no-treatment (1.29 ± 0.75%, 0.04 ± 0.03 g/mm$^3$), MDP (1.08 ± 0.16%, 0.03 ± 0.01 g/mm$^3$), and MDP-DOPA (1.23 ± 0.22%, 0.05 ± 0.01 g/mm$^3$) groups showed very few mineral deposits in the defect area. Both the no-treatment (4 weeks: 1.93 ± 1.34%, 0.15 ± 0.14 g/mm$^3$, 8 weeks: 3.25 ± 1.29%, 0.21 ± 0.10 g/mm$^3$) and the MDP scaffold (4 weeks: 4.08 ± 4.05%, 0.21 ± 0.12 g/mm$^3$, 8 weeks: 5.16 ± 3.41%, 0.32 ± 0.10 g/mm$^3$) groups showed small amounts of minerals deposited in the defect margin area at 4 and 8 weeks. However, the MDP-DOPA scaffold group (4 weeks: 14.82 ± 2.89%, 0.63 ± 0.03 g/mm$^3$, 8 weeks: 20.20 ± 3.40%, 0.62 ± 0.09 g/mm$^3$) showed significantly superior BV/TV and BMD results compared to the other groups. The MDP-DOPA scaffolds revealed accelerated bone mineralization at the early stage and much thicker bone formation at the defect area in the 3D and soft X-ray images at the late stage. After 8 weeks, we performed histological analysis using Goldner's trichrome staining to investigate bone regenerated at the defect area at the microscopic level (Fig. 4D to F). The no-treatment group only formed fibrotic tissue and were not measured any value of bone formation area and bone density in defect area. The defect area in the MDP group was surrounded by fibrotic tissue and a few bone spicules were deposited. Also, a very small regenerated bone formation area (0.80 ± 0.89%) and low bone density were observed (0.74 ± 0.51%). The MDP-DOPA (50.27 ± 22.31%) group showed that the newly formed bone area was highly integrated with the DOPA-coated layer and host bone. Moreover, the MDP-DOPA group (45.08 ± 19.22%) showed more compact bone density and had a similar bone density as that of the host bone. These results indicate that the number of cells recruited by the materials could be the same, but the

high number of host cells attached to the MDP-DOPA scaffold was able to form mineral deposits in the defect area in the early stage due to the synergetic effect between M2 polarization and CPP properties, consistent with the in vitro osteogenic differentiation test results.

### 3.5. *In vivo ectopic bone formation on implanted MDP and MDP-DOPA scaffolds in mice hindlimbs*

To investigate the ability of the cells recruited by the MDP and MDP-DOPA scaffolds to induce host cell recruitment and mineral deposition through osteogenic differentiation, we treated mice calvarial defects with both scaffolds for 1 and 2 weeks, retrieved the scaffolds from the calvarial defects, and transplanted them into mice hindlimb muscles for 2 and 4 weeks to analyze mineral deposition using live micro-CT (Fig. 5A). In the case of the MDP scaffold, no mineral deposits were detected in the soft X-ray or 3D images through live micro-CT analysis regardless of the MDP scaffold treatment period (Fig. 5B and C). However, the MDP-DOPA scaffold showed obvious differences according to the treatment period. The MDP-DOPA scaffold used to treat mouse calvarial defects for 1 week (BV/TV; 2 weeks: 0.08 ± 0.06%, 4w: 0.41 ± 0.37%, BMD; 2 weeks: 0.05 ± 0.02 g/mm$^3$, 4 weeks: 0.13 ± 0.05 g/mm$^3$) showed small amounts of minerals deposited at 2 and 4 weeks, but the MDP-DOPA scaffold used to treat mouse calvarial defects for 2 weeks (BV/TV; 2w: 0.33 ± 0.25%, 4w: 0.73 ± 0.63%, BMD; 2w: 0.24 ± 0.06 g/mm$^3$, 4w: 0.41 ± 0.15 g/mm$^3$) clearly showed implanted scaffolds in the soft X-ray images and robust mineral deposits, which mostly covered the surface of the implanted scaffolds (Fig. 5D and E). The in vitro LIVE/DEAD and CCK-8 assays results indicated that the host cells recruited by the bioactive peptides of casein in the early stage were highly attached to the MDP-DOPA scaffold in the calvarial defect area compared to the MDP scaffold. The results suggest that the bone regeneration efficacy was affected by cell recruitment, which depended upon the material treatment time in the defect area, initial cell attachment on the scaffolds, and the proper environment for osteogenic differentiation. After 2 and 4 weeks, histological analysis was performed on the samples retrieved from mice hindlimbs using Goldner's trichrome, Von Kossa staining, and OCN immunofluorescence staining (Fig. 5F and G). The quantification results and numerical OCN staining values were added to Fig. S8. Consistent with the live micro-CT results, the MDP scaffold was surrounded only by connective tissue and small amounts of deposited minerals were observed nearby, whereas the MDP-DOPA scaffold with a treatment period of 1 week showed immature bone formation at 2 and 4 weeks. However, at 4 weeks, the newly formed mature bone was strongly integrated with the surface of the scaffolds treated for 2 weeks.

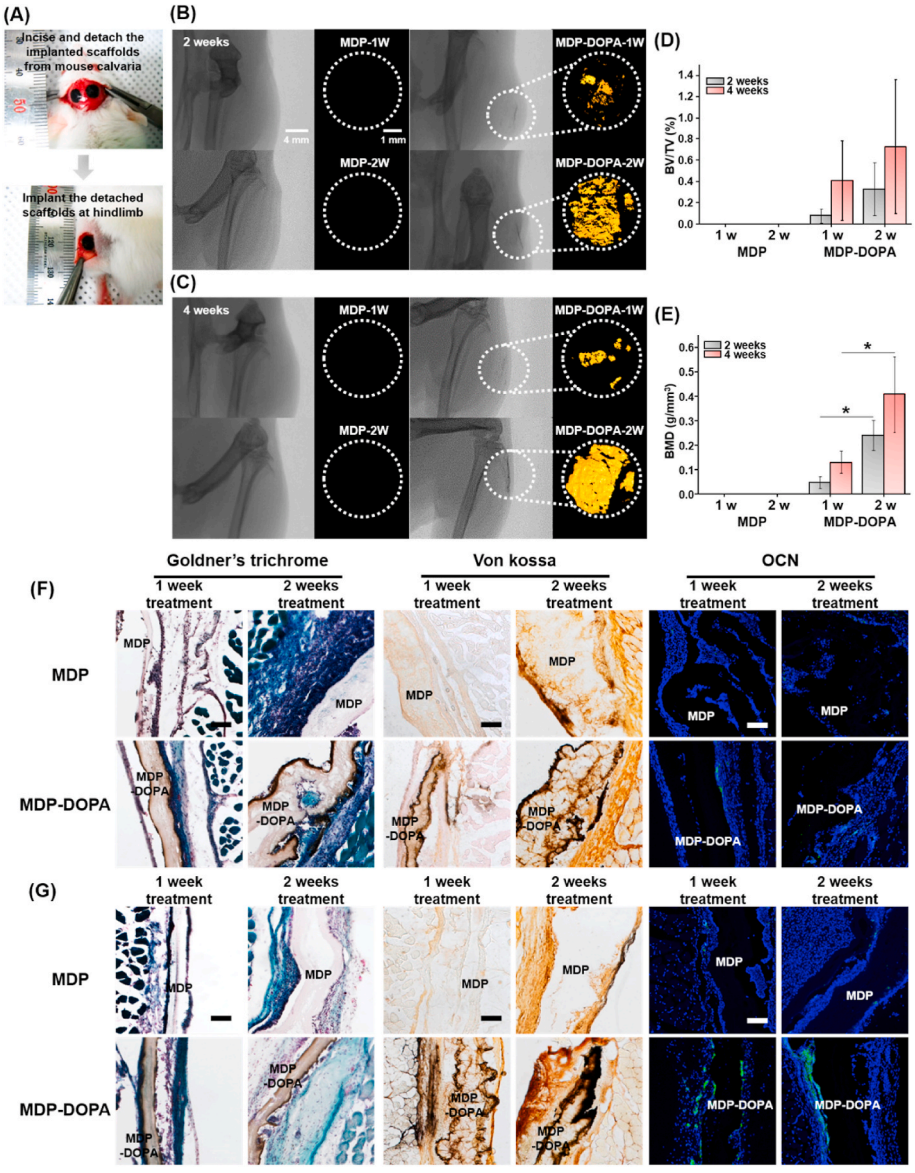


**Fig. 5.** In vivo mouse ectopic bone formation study. (A) The preparation procedure of ectopic bone formation model (n = 10/per group, each experiment). Live micro-CT analysis was progressed to examine rate of mineral deposition at implantation site for (B) 2 and (C) 4 weeks. At each time points, (D) BV/TV and (E) BMD of MDP and MDP-DOPA groups were measured ($p^* < 0.05$). After 4 weeks, histological analyses were performed. Representative images of Goldner's trichrome, Von kossa and immunohistochemical staining for (F) 2 weeks and (G) 4 weeks (Scale bar = 100 μm).

### 3.6. Identification of phenotype and cytokines secreted from macrophages recruited in the early stage in the mouse calvarial defect model

We had demonstrated the induction of macrophage recruitment toward both MDP and MDP-DOPA scaffolds, which improved the osteogenic differentiation of bmMSCs by the cytokines secreted from macrophages and CPP in the scaffolds in vitro and in vivo. For a more detailed understanding of the response of macrophages to both the MDP and MDP-DOPA scaffolds, we investigated the specific phenotypes and cytokines secreted from recruited macrophages in the early stage using the mouse calvarial defect model (Fig. 6). After 1 week, we retrieved scaffolds and stained them for F4/80, CD44, and ALP, which indicate macrophages, mesenchymal stem cells, and early osteogenic markers, respectively. The quantification results and numerical F4/80, CD44 and ALP staining values were added to Fig. S9. Both the MDP and MDP-DOPA scaffolds showed higher F4/80-positive signals around the scaffold materials than the no-treatment group (Fig. 6A). Accordingly, the MDP-DOPA scaffold showed high expressions of CD44 and ALP compared to the no-treatment and MDP scaffold groups (Fig. 6B and C). We confirmed that both the MDP and MDP-DOPA scaffolds could recruit more macrophages than the no-treatment group due to the presence of β-casochemotide-1. However, the number of recruited MSCs was significantly different between the MDP and MDP-DOPA scaffolds because of the cellular adhesion rate influenced by the surface characteristics. Because of this distinct difference, osteogenic differentiation in the host could progress rapidly, as we confirmed in the in vivo orthotopic bone formation study. Fig. 6D to F shows the predominant phenotypes of the recruited macrophages in each material implant area using CD86 and CD206 antibodies, which are M1 and M2 macrophage markers, respectively. The no-treatment group showed similar amounts of uniformly distributed M1 (3.62 ± 1.33%) and M2 (2.94 ± 1.01%) macrophages in the defect areas. In the case of the MDP scaffold, positive CD86 signals (9.68 ± 1.97%) were highly expressed compared to the expression of CD206 (1.16 ± 0.37%). In contrast to the MDP scaffold, CD206-positive signals (6.78 ± 0.98%) were increased compared to the expression of CD86 (4.56 ± 1.68%) in the MDP-DOPA scaffold. These results could indicate that accelerated bone regeneration because macrophages plays a crucial role in inducing the healing of damaged tissues by the secretion of various cytokines [1]. Related to these results, we analyzed which cytokines were predominantly secreted by the MDP and MDP-DOPA scaffolds in the defect sites in the early stage (Fig. 6G to I). The cytokines secreted in the MDP group were primarily pro-inflammatory cytokines such as CCL5, CXL16, G-CSF, IFNγ, and others compared to the MDP-DOPA group. In the early stage, the MDP group dominantly recruited M1 phenotype macrophages, which secreted pro-inflammatory cytokines, and this event led to a prolonged

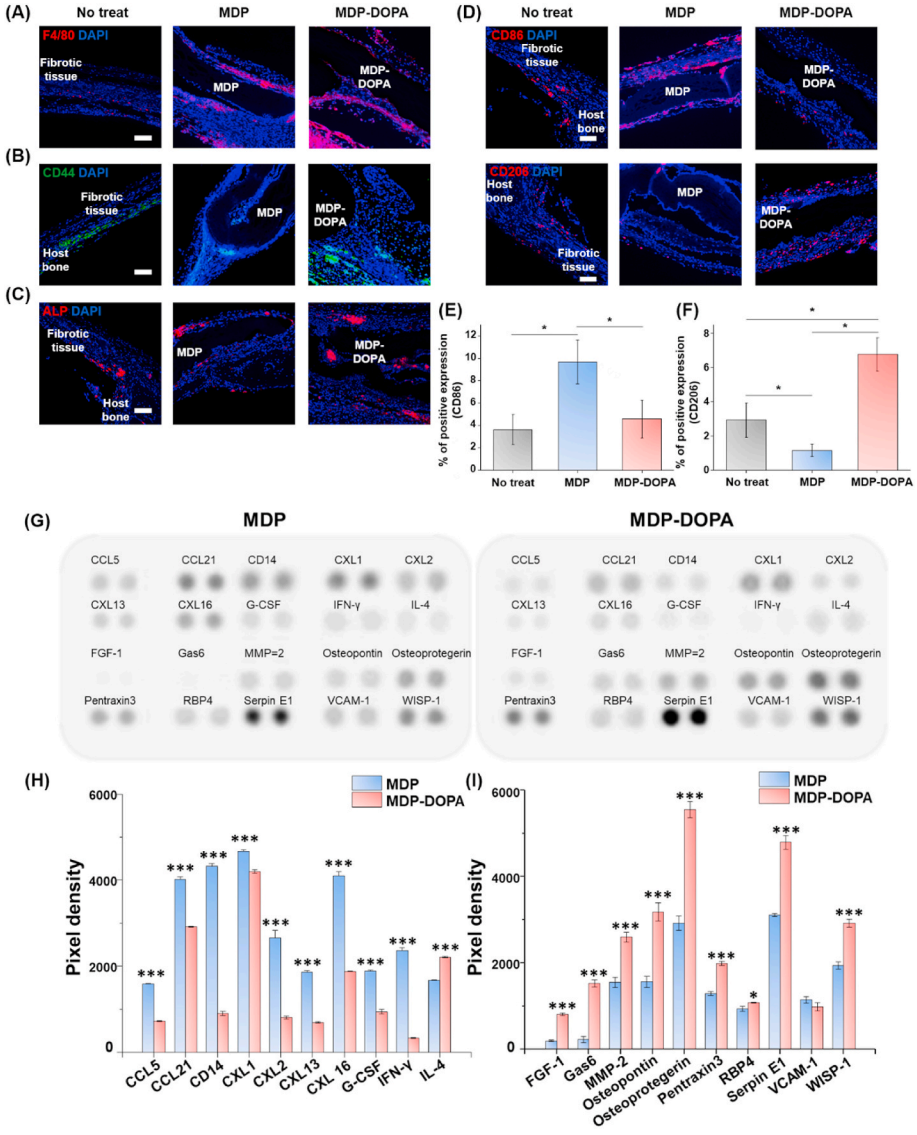


**Fig. 6.** After 1 week, implanted samples (n = 10/per group) were retrieved from mouse calvarial defect. Retrieved samples were performed immunohistochemical analysis using (A) F4/80, (B) CD44, (C) ALP, (D) CD86 and CD206 antibodies (Scale bar = 100 μm). Quantification of (E) CD86 and (F) CD206 positive cell ($p^* < 0.05$). Cytokine array assay of implanted MDP and MDP-DOPA scaffolds in calvarial defect. (G) Representative images of array membranes blot corresponding to MDP and MDP-DOPA scaffolds (n = 5/per group). Quantification of pixel density of (H) immune responds related marker and (I) osteogenic regeneration related marker.

inflammatory response that inhibited the next regeneration phase. The MDP-DOPA group mainly secreted bone repair-related cytokines such as FGF1, OPN, osteoprotegerin, and others compared to the MDP group. These results suggest that the MDP-DOPA group induced sequential events including the recruitment of M2 phenotype macrophages by β-casochemotide-1, the secretion of various cytokines for tissue repair, improvement in osteogenic differentiation, and mineral deposition by CPP, which led to accelerated bone regeneration.

## 4. Conclusion

We fabricated milk protein-based bioactive scaffolds through simple physical cross-linking between casein and PVA, which rapidly recruited macrophages toward the defect area in the early stage and played a crucial role in bone regeneration by the cytokines they secreted. We modified the surface of the MDP scaffold using DOPA to improve cell adhesion and confirmed that the process of surface modification did not induce surface deformation. In macrophage recruitment analyses, we showed that the bioactive MDP and MDP-DOPA scaffolds were able to accumulate macrophages in vitro and in vivo tests. Our cell behavior results showed that RAW 264.7 cells on the MDP-DOPA scaffold secreted M2 phenotype-associated proteins including BMP-2 and also promoted the osteogenic differentiation of bmMSCs treated with MDP-DOPA scaffold conditioned media. In addition, the MDP-DOPA scaffold group showed mineral deposits in the mouse calvarial defect model in live micro-CT, histological, immunohistochemical, RT-PCR, and cytokine array analyses. Furthermore, we confirmed that the implanted MDP and MDP-DOPA scaffolds rapidly recruited many macrophages in the early stage compared to the no-treatment group, but the MDP-DOPA scaffolds accumulated predominantly M2-phenotype macrophages. We demonstrated that the MDP-DOPA scaffold could provide beneficial effects for bone regeneration through the serial events of its bioactive peptides. The bioactive MDP-DOPA scaffold was shown to overcome some of the limitations of the existing scaffolds in the field of bone tissue engineering. Our unique and versatile MDP-DOPA scaffold suggests possible applications in tissue engineering platforms without the use of drugs or chemical agents.

## Ethics approval and consent to participate

The participants provided their written informed consent to participate in this study. All experimental protocols were approved by Center for Bio-medical Engineering Core Facility and ethics committee, the Institutional Animal Care and Use Committee at Dankook University (DKU-20-022).

## CRediT authorship contribution statement

**Min Suk Lee:** Writing – original draft, Writing – review & editing, Investigation, Formal analysis, Validation, Visualization, Funding acquisition. **Jin Jeon:** Writing – original draft, Investigation, Validation. **Sihyeon Park:** Investigation. **Juhan Lim:** Investigation. **Hee Seok Yang:** Conceptualization, Project administration, Supervision, Writing – review & editing.

## Declaration of interest

The authors declare that they have no known competing financial interests or personal relationships that could have appeared to influence the work reported in this paper.

## Acknowledgments

This research was supported by the Basic Science Research Program through the National Research Foundation of Korea (NRF) funded by the Ministry of Education (2020R1A6A3A01098495, 2020R1A6A1A030 43283) and by the Bio & Medical Technology Development Program of the National Research Foundation (NRF) funded by the Korean government (MSIT) (2018M3A9E2023259). This research was supported by Basic Science Research Capacity Enhancement Project through Korea Basic Science Institute (National research Facilities and Equipment Center) grant funded by the Ministry of Education (2019R1A6C1010033).

## Appendix A. Supplementary data

Supplementary data to this article can be found online at https://doi.org/10.1016/j.bioactmat.2022.05.028.

## References

[1] M. Ansari, Bone tissue regeneration: biology, strategies and interface studies, Progress in biomaterials 8 (4) (2019) 223–237.
[2] A. Longoni, L. Knezevic, K. Schepers, H. Weinans, A. Rosenberg, D. Gawlitta, The impact of immune response on endochondral bone regeneration, NPJ Regenerative medicine 3 (2018) 22.
[3] R. Sridharan, A.R. Cameron, D.J. Kelly, C.J. Kearney, F.J. O'Brien, Biomaterial based modulation of macrophage polarization: a review and suggested design principles, Mater. Today 18 (6) (2015) 313–325.
[4] X. Sun, Z. Ma, X. Zhao, W. Jin, C. Zhang, J. Ma, L. Qiang, W. Wang, Q. Deng, H. Yang, J. Zhao, Q. Liang, X. Zhou, T. Li, J. Wang, Three-dimensional bioprinting of multicell-laden scaffolds containing bone morphogenic protein-4 for promoting M2 macrophage polarization and accelerating bone defect repair in diabetes mellitus, Bioact. Mater. 6 (3) (2021) 757–769.
[5] M. Croes, M.C. Kruyt, W.M. Groen, K.M.A. van Dorenmalen, W.J.A. Dhert, F. C. Oner, J. Alblas, Interleukin 17 enhances bone morphogenetic protein-2-induced ectopic bone formation, Sci. Rep. 8 (1) (2018) 7269.
[6] G.E. Glass, J.K. Chan, A. Freidin, M. Feldmann, N.J. Horwood, J. Nanchahal, TNF-alpha promotes fracture repair by augmenting the recruitment and differentiation of muscle-derived stromal cells, Proc. Natl. Acad. Sci. U. S. A. 108 (4) (2011) 1585–1590.
[7] C. Zeonobia, G. Hajishengallis, Basic biology and role of interleukin-17 in immunity and inflammation, Periodontol. 2000 69 (1) (2015) 142–159.
[8] Q.L. Ma, L. Fang, N. Jiang, L. Zhang, Y. Wang, Y.M. Zhang, L.H. Chen, Bone mesenchymal stem cell secretion of sRANKL/OPG/M-CSF in response to macrophage-mediated inflammatory response influences osteogenesis on nanostructured Ti surfaces, Biomaterials 154 (2018) 234–247.
[9] Z. Chen, X. Mao, L. Tan, T. Friis, C. Wu, R. Crawford, Y. Xiao, Osteoimmunomodulatory properties of magnesium scaffolds coated with beta-tricalcium phosphate, Biomaterials 35 (30) (2014) 8553–8565.
[10] Y. Huang, C. Wu, X. Zhang, J. Chang, K. Dai, Regulation of immune response by bioactive ions released from silicate bioceramics for bone regeneration, Acta Biomater. 66 (2018) 81–92.
[11] M. Lucarini, Bioactive peptides in milk: from encrypted sequences to nutraceutical aspects, Beverages 3 (4) (2017) 41.
[12] T.K. Glab, J. Boratynski, Potential of casein as a carrier for biologically active agents, Top. Curr. Chem. 375 (4) (2017) 71.
[13] R.T. Recio, N.P. Guerra, A. Torrado, L.H. Skibsted, Interaction between calcium and casein hydrolysates: stoichiometry, binding constant, binding sites and thermal stability of casein phosphopeptide complexes, Int. Dairy J. 88 (2019) 25–33.
[14] L. Qin, H. Dong, Z. Mu, Y. Zhang, G. Dong, Preparation and bioactive properties of chitosan and casein phosphopeptides composite coatings for orthopedic implants, Carbohydr. Polym. 133 (2015) 236–244.
[15] H. Kitazawa, K. Yonezawa, M. Tohno, T. Shimosato, Y. Kawai, T. Saito, J.M. Wang, Enzymatic digestion of the milk protein beta-casein releases potent chemotactic peptide(s) for monocytes and macrophages, Int. Immunopharm. 7 (9) (2007) 1150–1159.
[16] A. Memic, T. Colombani, L.J. Eggermont, M. Rezaeeyazdi, J. Steingold, Z.J. Rogers, K.J. Navare, H.S. Mohammed, S.A. Bencherif, Latest advances in cryogel Technology for biomedical applications, Advanced Therapeutics 2 (4) (2019), 1800114.
[17] F. Chu, D.T. Thornton, H.T. Nguyen, Chemical cross-linking in the structural analysis of protein assemblies, Methods 144 (2018) 53–63.
[18] A. Porzionato, S. Barbon, E. Stocco, D. Dalzoppo, M. Contran, E. De Rose, P. P. Parnigotto, V. Macchi, C. Grandi, R. De Caro, Development of oxidized polyvinyl alcohol-based nerve conduits coupled with the ciliary neurotrophic factor, Materials 12 (12) (2019).
[19] S.H. Kim, J.H. Lee, H. Hyun, Y. Ashitate, G. Park, K. Robichaud, E. Lunsford, S. J. Lee, G. Khang, H.S. Choi, Near-infrared fluorescence imaging for noninvasive trafficking of scaffold degradation, Sci. Rep. 3 (2013) 1198.
[20] S.W. Hsiang, C.C. Tsai, F.J. Tsai, T.Y. Ho, C.H. Yao, Y.S. Chen, Novel use of biodegradable casein conduits for guided peripheral nerve regeneration, J. R. Soc. Interface 8 (64) (2011) 1622–1634.
[21] A. Gorska, A. Krupa, D. Majda, P. Kulinowski, M. Kurek, W.P. Weglarz, R. Jachowicz, Poly(Vinyl alcohol) cryogel membranes loaded with resveratrol as potential active wound dressings, AAPS PharmSciTech 22 (3) (2021) 109.

[22] S. Chen, B. Bai, D.J. Lee, S. Diachina, Y. Li, S.W. Wong, Z. Wang, H.C. Tseng, C. C. Ko, Dopaminergic enhancement of cellular adhesion in bone marrow derived mesenchymal stem cells (MSCs), J. Stem Cell Res. Ther. 7 (8) (2017).
[23] M. Kim, W. Kim, G. Kim, Topologically micropatterned collagen and poly(epsilon-caprolactone) struts fabricated using the poly(vinyl alcohol) fibrillation/leaching process to develop efficiently engineered skeletal muscle tissue, ACS Appl. Mater. Interfaces 9 (50) (2017) 43459–43469.
[24] J. Burgain, J. Petit, J. Scher, R. Rasch, B. Bhandari, C. Gaiani, Surface chemistry and microscopy of food powders, Prog. Surf. Sci. 92 (4) (2017) 409–429.
[25] C. Gaiani, M. Mullet, E. Arab-Tehrany, M. Jacquot, C. Perroud, A. Renard, J. Scher, Milk proteins differentiation and competitive adsorption during spray-drying, Food Hydrocolloids 25 (5) (2011) 983–990.
[26] F. Xu, L. Zhong, C. Zhang, P. Wang, F. Zhang, G. Zhang, Novel high-efficiency casein-based P–N-containing flame retardants with multiple reactive groups for cotton fabrics, ACS Sustain. Chem. Eng. 7 (16) (2019) 13999–14008.
[27] Y. Li, X. Li, Z. Cao, Y. Xu, Y. Gong, X. Shi, Fabrication of uniform casein/CaCO3 vaterite microspheres and investigation of its formation mechanism, Cryst. Growth Des. 17 (12) (2017) 6178–6188.
[28] S. Park, M.S. Lee, J. Jeon, J. Lim, C.H. Jo, S.H. Bhang, H.S. Yang, Micro-groove patterned PCL patches with DOPA for rat Achilles tendon regeneration, J. Ind. Eng. Chem. 105 (2022) 352–364.
[29] M. Filippi, G. Born, M. Chaaban, A. Scherberich, Natural polymeric scaffolds in bone regeneration, Front. Bioeng. Biotechnol. 8 (2020) 474.
[30] J.M. Ino, P. Chevallier, D. Letourneur, D. Mantovani, C. Le Visage, Plasma functionalization of poly(vinyl alcohol) hydrogel for cell adhesion enhancement, Biomatter 3 (4) (2013).
[31] A.V. Janorkar, E.W. Fritz Jr., K.J. Burg, A.T. Metters, D.E. Hirt, Grafting amine-terminated branched architectures from poly(L-lactide) film surfaces for improved cell attachment, J. Biomed. Mater. Res. B Appl. Biomater. 81 (1) (2007) 142–152.
[32] L. Vi, G.S. Baht, H. Whetstone, A. Ng, Q. Wei, R. Poon, S. Mylvaganam, M. Grynpas, B.A. Alman, Macrophages promote osteoblastic differentiation in-vivo: implications in fracture repair and bone homeostasis, J. Bone Miner. Res. : the official journal of the American Society for Bone and Mineral Research 30 (6) (2015) 1090–1102.
[33] M. Wang, F. Chen, J. Wang, X. Chen, J. Liang, X. Yang, X. Zhu, Y. Fan, X. Zhang, Calcium phosphate altered the cytokine secretion of macrophages and influenced the homing of mesenchymal stem cells, J. Mater. Chem. B 6 (29) (2018) 4765–4774.
[34] Y. Zhu, Z. Ma, L. Kong, Y. He, H.F. Chan, H. Li, Modulation of macrophages by bioactive glass/sodium alginate hydrogel is crucial in skin regeneration enhancement, Biomaterials 256 (2020), 120216.
[35] P. Qiu, M. Li, K. Chen, B. Fang, P. Chen, Z. Tang, X. Lin, S. Fan, Periosteal matrix-derived hydrogel promotes bone repair through an early immune regulation coupled with enhanced angio- and osteogenesis, Biomaterials 227 (2020), 119552.
[36] O.R. Mahon, D.C. Browe, T. Gonzalez-Fernandez, P. Pitacco, I.T. Whelan, S. Von Euw, C. Hobbs, V. Nicolosi, K.T. Cunningham, K.H.G. Mills, D.J. Kelly, A. Dunne, Nano-particle mediated M2 macrophage polarization enhances bone formation and MSC osteogenesis in an IL-10 dependent manner, Biomaterials 239 (2020), 119833.
[37] C.R. Nuttelman, D.J. Mortisen, S.M. Henry, K.S. Anseth, Attachment of fibronectin to poly(vinyl alcohol) hydrogels promotes NIH3T3 cell adhesion, proliferation, and migration, J. Biomed. Mater. Res. 57 (2) (2001) 217–223.
[38] Q. Li, A. Shen, Z. Wang, Enhanced osteogenic differentiation of BMSCs and M2-phenotype polarization of macrophages on a titanium surface modified with graphene oxide for potential implant applications, RSC Adv. 10 (28) (2020) 16537–16550.
[39] L. Pang, Y. Shen, H. Hu, X. Zeng, W. Huang, H. Gao, H. Wang, D. Wang, Chemically and physically cross-linked polyvinyl alcohol-borosilicate gel hybrid scaffolds for bone regeneration, Materials science & engineering, C, Materials for biological applications 105 (2019), 110076.
[40] T. Zhou, S. Chen, X. Ding, Z. Hu, L. Cen, X. Zhang, Fabrication and characterization of collagen/PVA dual-layer membranes for periodontal bone regeneration, Front. Bioeng. Biotechnol. 9 (2021), 630977.
[41] C. Gao, Q. Gao, Y. Li, M.N. Rahaman, A. Teramoto, K. Abe, Preparation and in vitro characterization of electrospun PVA scaffolds coated with bioactive glass for bone regeneration, J. Biomed. Mater. Res. 100 (5) (2012) 1324–1334.
[42] B.M. Donida, E. Mrak, C. Gravaghi, I. Villa, S. Cosentino, E. Zacchi, S. Perego, A. Rubinacci, A. Fiorilli, G. Tettamanti, A. Ferraretto, Casein phosphopeptides promote calcium uptake and modulate the differentiation pathway in human primary osteoblast-like cells, Peptides 30 (12) (2009) 2233–2241.